Nano Research

ISSN 1998-0124 CN 11-5974/O4
https://doi.org/10.1007/s12274-023-6127-7

Research Article

Investigation of MXene nanosheets based radio-frequency electronics by skin depth effect

Rongguo Song[1,2,§], Yunfa Si[3,§], Wei Qian[2], Haoran Zu[2], Bilei Zhou[1], Qinglei Du[1], Daping He[2] (✉), and Yongliang Wang[1] (✉)

[1] *Air Force Early Warning Academy, Wuhan 430019, China*
[2] *Hubei Engineering Research Center of RF-Microwave Technology and Application, Wuhan University of Technology, Wuhan 430070, China*
[3] *Hainan Research Institute, Wuhan University of Technology, Sanya 572000, China*
[§] *Rongguo Song and Yunfa Si contributed equally to this work.*

Received: 3 August 2023 / **Revised:** 24 August 2023 / **Accepted:** 25 August 2023

ABSTRACT

Various new conductive materials with exceptional properties are utilized for the preparation of electronic devices. Achieving ultra-high conductivity is crucial to attain excellent electrical performance. However, there is a lack of systematic research on the impact of conductor material thickness on device performance. Here, we investigate the effect of conductor thickness on power transmission and radiation in radio-frequency (RF) and microwave electronics based on MXene nanosheets material transmission lines and antennas. The MXene transmission line with thickness above the skin depth exhibits a good transmission coefficient of approximately −3 dB, and the realized gain of MXene antennas exceeds 2 dBi. Additionally, the signal transmission strength of MXene antenna with thickness above the skin depth is higher than 5-μm MXene antenna approximately 5.5 dB. Transmission lines and antennas made from MXene materials with thickness above the skin depth exhibit stable and reliable performance, which has significant implications for obtaining high-performance RF and microwave electronics based on new conductive materials.

KEYWORDS

MXene film, radiao-frequency electronics, antenna, transmission line, skin depth

1 Instruction

In the fields of Internet of Things (IoT) [1, 2], Internet of Vehicles (IoV) [3, 4], and body area network (BAN) [5, 6] wireless communication systems, billions of antennas and other radio-frequency (RF) and microwave electronics [11] serve as the eyes for information exchange through WiFi [7], bluetooth [8], and radio frequency identification (RFID) [9, 10]. In the past, in order to achieve excellent electrical performance, metal materials such as copper and gold with high conductivity are used to manufacture wireless communication devices [12, 13]. Nevertheless, the unsatisfactory intrinsic properties of metal materials (i.e., large density, high rigidity, and susceptibility to corrosion) can not meet new functional requirements under many situations of new electronic devices, especially flexible electronics [14]. In addition, with the explosive growth of electronic products, the environmental pressure caused by electronic waste is becoming increasingly severe [15, 16]. With advancements in material processing technology, various lightweight and flexible materials with high conductivity have been developed, such as graphene [17, 18], MXene [19], carbon nanotubes [20, 21], etc., leading to tremendous efforts focused on developing new material-based wireless communication devices that can substitute metals [22–26].

The morphology, conductivity and thickness of conductor materials profoundly affect the electrical behavior of wireless communication electronics. Commonly employed engineering forms include conductive films or ink which can be carved or printed to facilitate batch preparation of electronics [27–30]; however, processing microscopic materials such as powders and nanosheets into macroscopic electronic devices poses challenges due to their inherent characteristics. In our previous work, we explored the impact of material conductivity on the performance of RF and microwave electronics and proposed the relationship between material conductivity and conductor loss [31]. In addition, the thickness of conductor materials is also related to the electrical behavior of wireless communication devices. In the RF field, the current in the conductor is only transmitted within a certain thickness of the conductor material surface, that is, the skin effect [32]. This special thickness is defined as skin depth, which closely relates to conductor material conductivity and operating frequency in wireless communication devices. Therefore, designing conductor material thickness plays an essential role in determining electrical behavior in electronic devices. While many works have focused on improving conductivity to enhance electrical behavior in electronic devices, few reports have investigated how conductor material thickness affects device performance along this dimension.

Herein, we investigate the impact of conductor thickness based on MXene nanosheets film on performances of RF and microwave electronics. The conductivity of MXene film is 1.2 ×

Address correspondence to Daping He, hedaping@whut.edu.cn; Yongliang Wang, ylwangkjld@163.com

10^5 S/m, and six different thicknesses (5, 9, 15, 21, 29, and 40 μm) are fabricated by controlling the coating thickness during film formation. To examine the effect of conductor material thickness on RF power transmission, six microstrip transmission lines made from MXene materials with varying thicknesses were prepared. T5 and T6 MXene transmission lines exhibit good transmission coefficients (−3 dB) exceeding skin depth (24.57 μm @ 3.5 GHz), which are much higher than that of T1 MXene transmission line (−15.42 dB). As the thickness increases, the efficiency of the transmission line gradually improves until it stabilizes above skin depth. We also investigated radiation performance using MXene antennas operated at 3.5 GHz with different thicknesses. The realized gain for T5 and T6 MXene antennas exceeds 2 dBi exceeding skin depth and is approximately 5.56 dB higher than that for T1 Mxene antenna. The signal strength for T5 and T6 MXene antennas is about 5.5 dB stronger than that for the T1 MXene antenna as well. As such our research demonstrates that the thickness of conductor material has a significant impact on RF and microwave electronics' performance. To achieve optimal device functionality, conductor materials require greater thickness compared to skin depth.

2 Experimental

2.1 Fabrication of MXene film

The MXene flakes were synthesized through the minimally intensive layer delamination (MILD) method by etching Ti_3AlC_2 MAX powders [33]. In the first step, 3.2 g of LiF powders were dissolved in a polytetrafluoroethylene (PTFE) container containing 40 mL of 9 M HCl. After that, 2 g of MAX powders was gradually added into the etching solution and etched at 50 °C for 24 h. Subsequently, the etching solution underwent multiple washes with deionized water until self-delamination occurred at a supernatant pH of 5–6. Finally, the MXene nanosheets were obtained by centrifuging the supernatant at 9000 rpm for 15 min. The resulting MXene sediment was diluted to 30 mg/mL for use in subsequent steps.

To begin with, the MXene ink was applied onto a Celgard 3501 substrate using a blade coating process, forming MXene gel films. Following this, the films were left to dry overnight at room temperature. Ultimately, the dried MXene films could be easily peeled off from the substrate. The thickness of the MXene films could be regulated by adjusting the scraper height during the blade coating process.

2.2 Fabrication and measurement of MXene electronics

The MXene microstrip transmission line and antenna were manufactured by laser engraving method [34]. Firstly, the MXene film was cut by laser engraving machine (LPKF Protolaser U4) according to the designed electronics structure. Then, the MXene structures were combined to the dielectric substrate (FR4 and Rogers 5880) to form MXene electronics. The MXene microstrip transmission line was measured by vector network analyzer (VNA, Keysight N5247A). Two coaxial cables were used to connect VNA and both ends of the MXene transmission line to test the transmission coefficient. The performances of MXene antenna were measured by VNA and antenna measurement system. The gain of antenna was measured by three-antenna method. The signal transmission performances of MXene antenna were measured by a signal generator (Keysight E8267D), signal analyzer (Keysight N9010A), and receiving horn antenna. All performances of MXene electronics were measured in microwave anechoic chamber.

2.3 Materials characterization

X-ray diffractometer (XRD) patterns were acquired using a Bruker D8 Advance diffractometer, employing Cu Kα radiation with a wavelength (λ) of 0.1541 nm. Raman spectra were recorded utilizing a LabRam HR Evolution Confocal laser Raman instrument. A Thermo Scientific Escalab 250 X-ray photoelectron spectroscopy (XPS) was employed to determine the elemental compositions of the samples. Scanning electron microscope (SEM) images were captured using a ZEISS Gemini electron microscopy 300.

3 Results and discussion

3.1 Characterization of MXene film

Figure 1(a) presents a schematic representation of the process involved in the preparation of MXene films. For the first step, the Ti_3AlC_2 MAX phase powders were etched 24 h in the etching solution at 50 °C. This process can remove the "Al" atom layer from the Ti_3AlC_2 MAX and get the accordion-like multi-layer MXene (Figs. S1 and S2 in the Electronic Supplementary Material (ESM)). Subsequently, wash multi-layer MXene through centrifugation until the pH is approximately 6. Then, the MXene ink shown in the photograph containing single-layer MXene was obtained through manual shaking the multi-layer MXene. Next, the MXene ink has been directly coated on the Celgard 3501 substrate using the simply blade-casting method. After drying, the MXene film can be easily peeled from the substrate. The relatively smooth surface of MXene film with less wrinkle has been shown in Fig. 1(b), thanks to the single layer MXene flakes with a clean surface and large lateral dimensions (Fig. 1(c)). Meanwhile, Fig. 1(d) measured the thickness of MXene nanosheets is 1.25 nm, which proves the successful preparation of single-layer flakes.

The XRD pattern (Fig. 1(e)) displays a prominent (200) peak at ~ 6.5° in the MXene films, and the distinct (104) characteristic peak has disappeared, confirming the successful preparation of MXene [35]. Furthermore, this observation is also supported by the Raman spectrum in Fig. 1(f). The 203 and 717 cm^{-1} peaks represent the Ti–C and C–C vibrations (A_{1g}), and the absorption peaks at 287, 380, 591, and 626 cm^{-1} are associated with the E_g vibrations, involving O, C and surface functional group atoms, which are consistent with previous reports [36]. The XPS analysis investigated the surface chemical state and composition of the MXene films. Figure S3 in the ESM displays distinct signals related to C, Ti, O and F elements, suggesting the absence of contamination during film preparation. There is no TiO_2 characteristic peak in high-resolution Ti 2p patterns, as shown in Fig. 1(g), manifesting that the MXene is not or less oxidized, which is beneficial for maintaining the conductivity during the testing process.

To investigate the impact of MXene film thickness on RF and microwave electronic performances, six different thicknesses of MXene films were prepared by controlling the height of the scraper (Fig. 2), which are 5 μm (T1), 9 μm (T2), 15 μm (T3), 21 μm (T4), 29 μm (T5), and 40 μm (T6), respectively. Simultaneously, the cross-sectional SEM images of MXene films also reveal compact layer-by-layer structures, and this is due to the MXene flakes can achieve uniform alignment by shear force and gravity-induced layer-by-layer assembly. Based on this structure, these MXene films can maintain the conductivity of stabilized ~ 1.2×10^5 S/m, as shown in Fig. S4 in the ESM.

3.2 Transmission performance of MXene transmission line

In contrast to direct current transmission methods where current is distributed across a conductor's entire cross-section, the power exhibit a skin effect causing current concentration near its surface

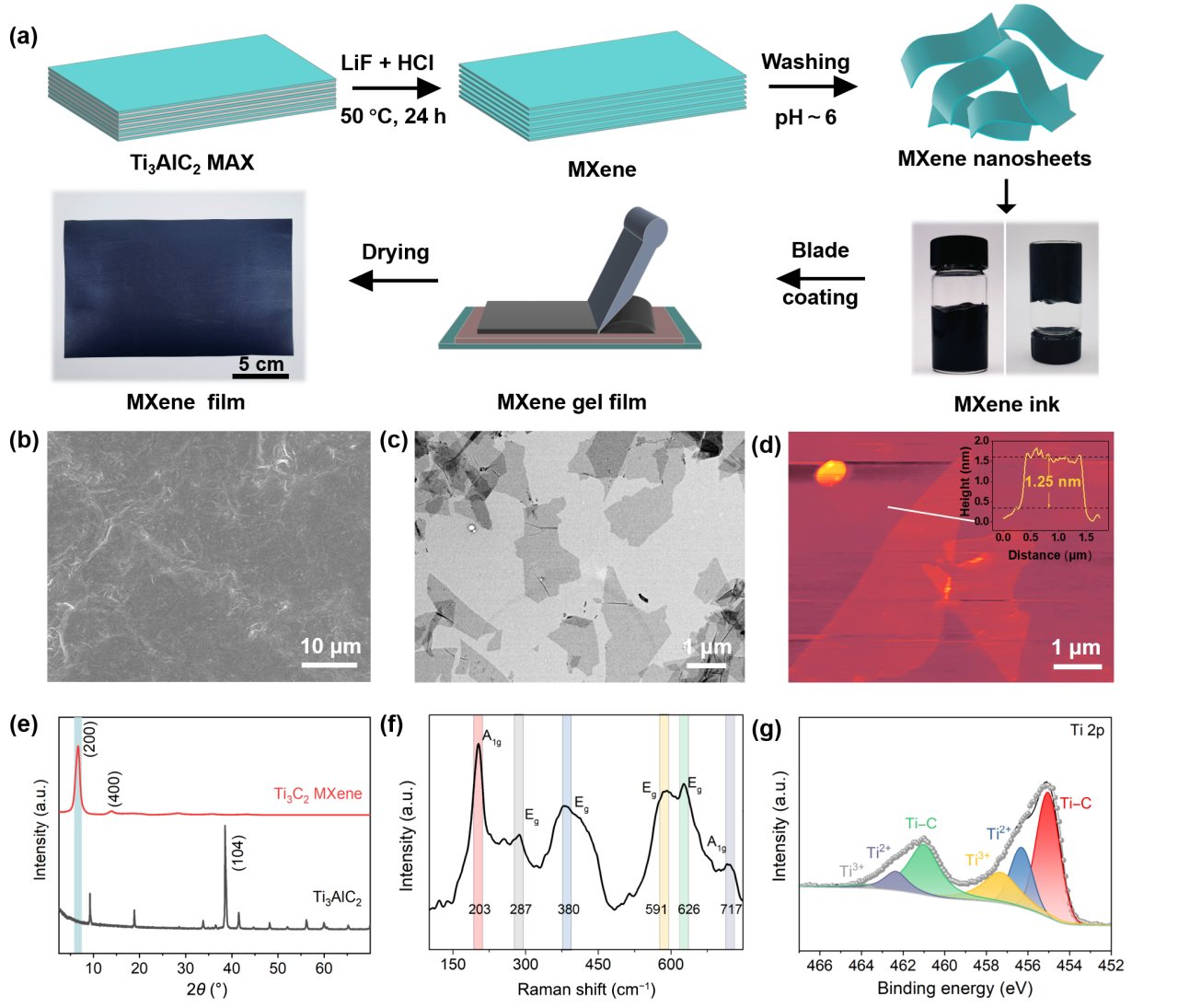

Figure 1 Fabrication and characterization of the MXene film. (a) The fabrication process of MXene film. (b) SEM image of the MXene film surface. (c) TEM image and (d) AFM image of MXene nanosheets. (e) XRD patterns, (f) Raman spectrum, and (g) high-resolution Ti 2p pattern of MXene film.

at RF and microwave frequencies. The skin depth characterizes electromagnetic wave energy transmission thickness on a conductor's surface intricately linked to its conductivity and operating frequency. The skin depth (δ) is calculated as

$$\delta = \frac{1}{\sqrt{\pi f \mu \sigma}} \quad (1)$$

where f is the working frequency, μ is the material permeability and σ is the conductivity of conductive material.

Figures 3(a) and 3(b) illustrate the calculation of skin depth as a function of working frequency and materials conductivity. As shown in Fig. 3(a), the skin depth decreases with the increase of material conductivity in the RFID frequency band (915 MHz), WiFi communication frequency band (2.45 GHz), and 5G communication frequency band (3.5 GHz). Under the same material conductivity, the lower the operating frequency, the greater the skin depth. Figure 3(b) shows the results of skin depth variation with working frequency under different material conductivity (10^2–10^6 S/m). The conductivity of common new conductive materials is listed in Table S1 in the ESM. Taking the working frequency of 3.5GHz as an example, the skin depth is 851.15 μm (10^2 S/m), 269.15 μm (10^3 S/m), 85.11 μm (10^4 S/m), 26.91 μm (10^5 S/m), and 8.51 μm (10^6 S/m) under different material conductivity, which proves that increasing conductivity is an effective method to reduce skin depth.

To investigate the effect of skin depth on the performance of RF energy transmission, a microstrip transmission line is designed, as shown in Fig. 3(c) and Fig. S5 in the ESM. The transmission line is designed on 0.787-mm-thick Rogers 5880 with dielectric constant of 2.2 and loss tangent 0.0009. The dimensions of transmission line and ground are 100 mm × 1.6 mm and 100 mm × 30 mm, respectively. According to the model, a variety of microstrip transmission line prototypes were fabricated based on MXene film materials. 5 μm (T1), 9 μm (T2), 15 μm (T3), 21 μm (T4), 29 μm (T5), and 40 μm (T6) MXene films are used to fabricate the microstrip transmission line prototypes, as shown in Fig. S6 in the ESM. The dimensions of the MXene transmission line are cut using an LPKF Proteaser U4 with accuracy of 20 μm. The substrate and metal ground layer of all prototypes are the same. By keeping all physical profile and materials the same except of the thickness of the microstrip transmission line, the electromagnetic energy transmission characteristics of MXene microstrip transmission lines can be directly explored. The transmission coefficient and reflection confficient of each MXene transmission line were measured by a Keysight N5247A vector network analyzer, as shown in Fig. 3(d) and Fig. S7 in the ESM. At the working frequency of 3.5 GHz, the skin depth is 24.57 μm as the conductivity of MXene film is 1.2 × 10^5 S/m, which indicates that the thickness of T5 and T6 MXene film material samples is greater than the skin depth, while the thickness of T1–T4 is less than the skin depth. It can be clearly seen from Fig. 3(d) that the T5 and T6

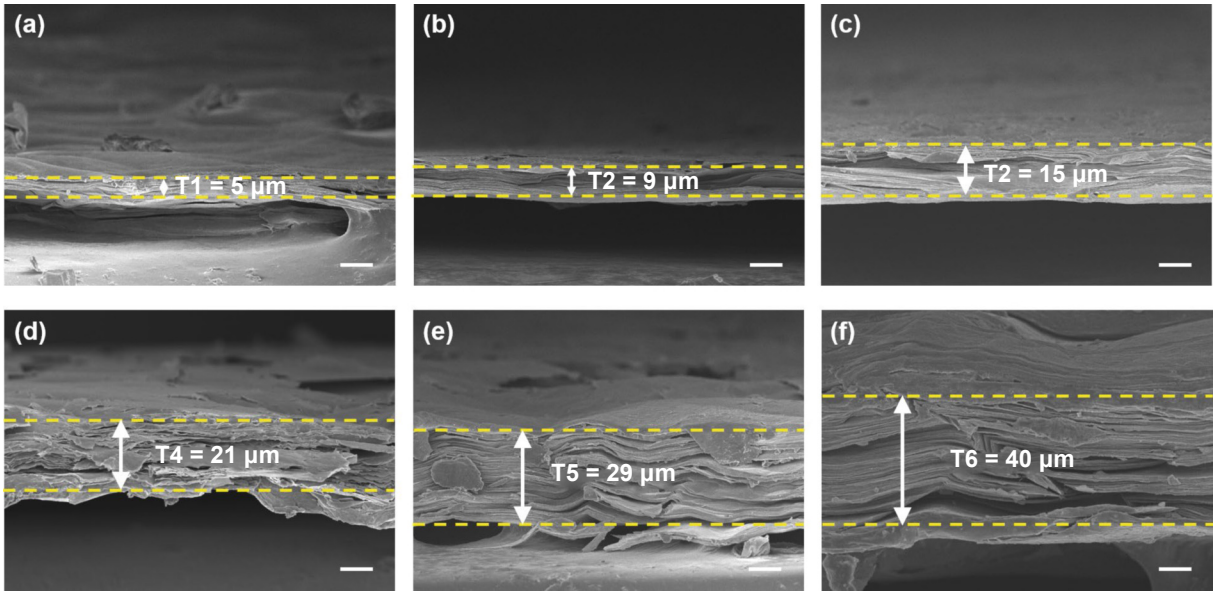

Figure 2 Cross-sectional SEM images of MXene film showing the thickness. (a) T1, 5 μm, (b) T2, 9 μm, (c) T3, 15 μm, (d) T4, 21 μm, (e) T5, 29 μm, and (f) T6, 40 μm. Scale bar, 10 μm.

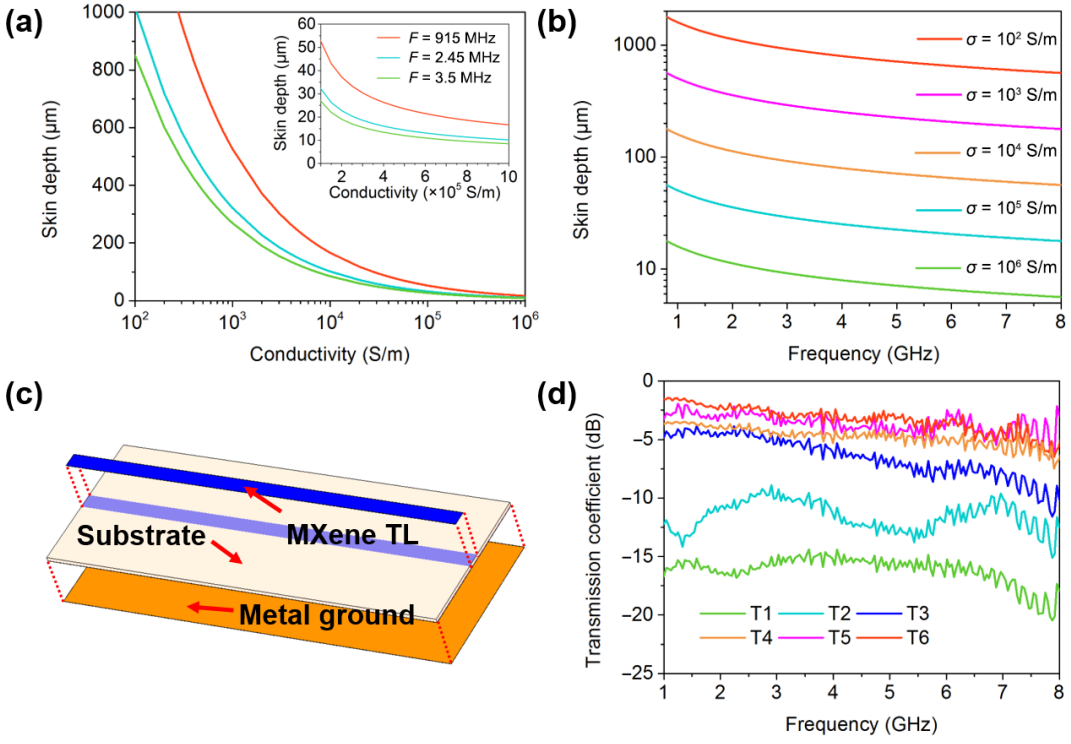

Figure 3 Skin depth and performance of MXene transmission line. (a) Skin depth at 915 MHz (red line), 2.45 GHz (blue line) and 3.5 GHz (green line) with different electrical conductivity. (b) Skin depth with conductivity of 10^2 S/m (red line), 10^3 S/m (purple line), 10^4 S/m (orange line), 10^5 S/m (blue line), and 10^6 S/m (green line) at different frequency. (c) Digital photo of MXene microstrip transmission line. (d) Measured transmission coefficient of MXene microstrip transmission line.

MXene transmission line prototypes have good and similar transmission coefficients (~ −3 dB). The thickness of T3 and T4 Mxene film material samples is slightly smaller than the skin depth, so the transmission coefficient of their transmission line prototypes is slightly worse than that of T5 and T6 transmission line prototypes. In addition, the thickness of T1 and T2 MXene film material samples is much smaller than the skin depth, resulting in severe degradation of their transmission line prototype performance. Especially for the T1 MXene film transmission line prototype, the transmission coefficient at 3.5 GHz is only −15.42 dB, which indicates that the transmission efficiency of T1 MXene film transmission line prototype is only ~ 6% of T5 and T6 MXene film transmission line prototype. As the frequency increases, at a working frequency of 7 GHz, the transmission coefficient of the T4 MXene film transmission line prototype exhibits similarity to those of the T5 and T6 MXene film transmission line prototypes due to T4 exceeding the skin depth (17.34 μm @ 7 GHz). Hence, the thickness of conductor materials exerts a substantial influence on the efficiency of electromagnetic energy transmission of RF and microwave electronics. To achieve optimal energy transfer efficiency, it is imperative to ensure that the thickness of the conductor material exceeds the skin depth.

3.3 Radiation performance of MXene antenna

To investigate the effect of conductor material on the performance of RF energy radiation, a microstrip antenna operating at 3.5 GHz is designed, as shown in Fig. 4(a) and Fig. S8 in the ESM. The antenna is designed on 1.6-mm-thick RF4 substrate with dielectric

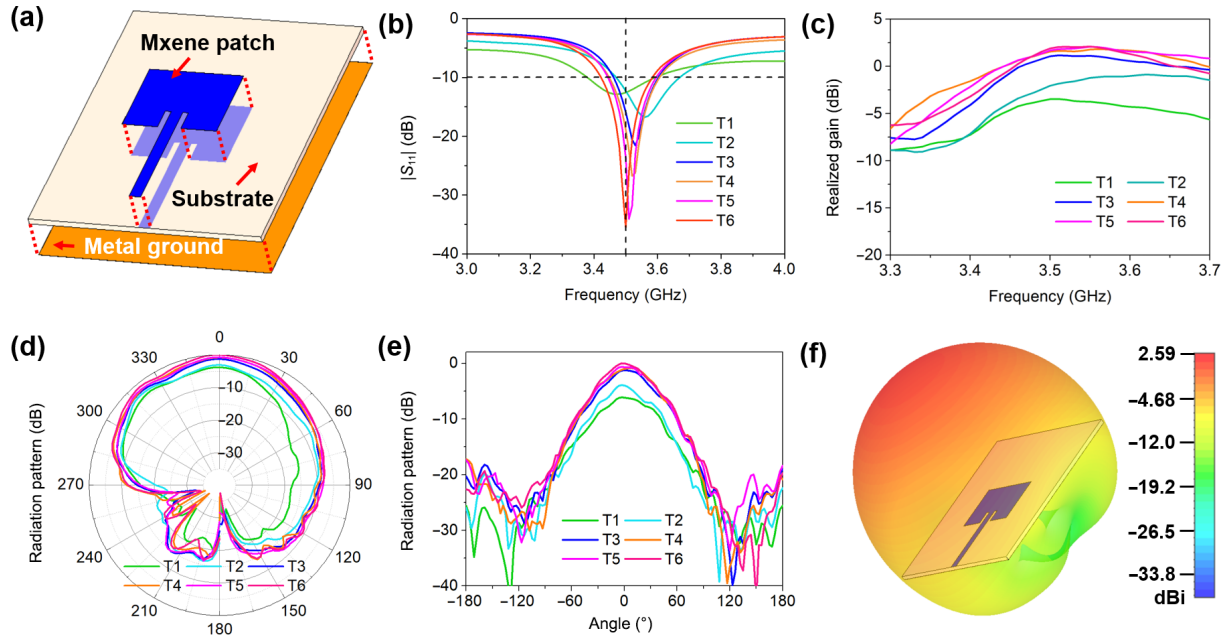

Figure 4 Performances of MXene antennas. (a) Physical structure of MXene antenna. (b) Reflection coefficient, (c) realized gain, and ((d) and (e)) radiation patterns of MXene antenna with thickness of T1–T6. (f) Simulated 3D radiation pattern of MXene antenna with thickness of T6.

constant of 4.3 and loss tangent 0.025. The dimensions of antenna patch is 24.44 mm × 19.76 mm. The antenna is fed by a microstrip line with the width of 2.98 mm. Moreover, the substrate and metal ground have the same dimensions of 75 mm × 30 mm. According to the model, a variety of MXene antenna prototypes (T1–T6) were fabricated, as shown in Fig. S9 in the ESM. The reflection coefficient of each MXene antenna was measured by a Keysight N5247A vector network analyzer, as depicted in Fig. 4(b). The T4 and T5 MXene antennas resonate at approximately 3.5 GHz with a reflection coefficient less than −20 dB (less than 1% energy reflects back to signal source), while the T1 and T2 MXene antennas have a reflection coefficient of about −12 dB at 3.5 GHz (6% energy reflects back to signal source). Additionally, the gain and radiation pattern of MXene antenna prototypes were measured using a standard antenna measurement system in an anechoic chamber (Fig. S8 in the ESM). Figure 4(c) illustrates the realized gain of the MXene antenna prototypes measured using the three-antenna method. The peak realized gains for T1, T2, T3, T4, T5, and T6 are −3.45, −0.87, 1.56, 1.78, 2.09, and 2.11 dBi, respectively (Fig. S9 in the ESM). The thickness of MXene film higher than skin depth leads to significant radiation performance improvement for antennas; thus there is an increase in realized gain from T1 MXene antenna to T6 MXene antenna by up to 5.56 dB. Figures 4(d) and 4(e) show that E-plane and H-plane radiation patterns normalized according to T6 MXene antenna exhibit half power beamwidths of 86° and 67°, respectively, which display typical microstrip antenna radiation patterns consistent with simulated results shown in Fig. 4(f). Furthermore, the measured normalized radiation patterns also demonstrate consistent results with those obtained from realized gain measurements for all six antennas (T1–T6); however, T1's radiation pattern is deformed indicating poor radiation capability. A minor difference between simulated and measured gains may be attributed potentially due to contact resistance between SubMiniature version A (SMA) connector and antenna.

To further illustrate the effect of conductor materials thickness on radiation performance, a series of signal transmission experiments were conducted. Figures 5(a)–5(g) depict the measured results of signal strength for the T1–T6 MXene antenna prototypes under identical source power conditions in an anechoic chamber (Fig. 5(h)). The MXene antenna is connected to the signal generator via a coaxial cable as the transmitting terminal, while a standard horn antenna is linked to the signal analyzer as the receiving terminal. The working frequency and power amplitude of the signal generator are set as 3.5 GHz and 0 dBm, respectively. A fixed distance of 2.5 m and the same height between each MXene antenna prototype and the horn antenna ensures that all signals experience equal path loss and maximum signal strength upon reaching the receiving terminal. Furthermore, prior to measurement, calibration and compensation were performed for cable loss (6.67 dB), as shown in Fig. S10 in the ESM. From these measured results, it becomes evident that T5 and T6 MXene antennas exhibit significantly higher and similar levels of signal strength (38.19 and −38.17 dBm, respectively) compared to T1 and T2 MXene antennas (−43.74 and −41.28 dBm, respectively), indicating their capability for long-distance transmission. Moreover, as the thickness increases, the signal strength gradually increases until it stabilizes when the thickness beyond the skin depth. All measured results of MXene antenna demonstrate that conductor material thickness plays a crucial role in determining RF and microwave electronics radiation performance.

4 Conclusions

In summary, we have demonstrated that the thickness of conductor materials has a significant impact on the performance of RF electronics according to various MXene film materials with different thicknesses transmission line and antenna prototypes. When the conductor material thickness is below the skin depth, microstrip transmission lines exhibit poor power transmission efficiency. As the conductor material thickness increases, transmission efficiency gradually improves until it surpasses the skin depth and stabilizes. Furthermore, antennas based on MXene film with varying thicknesses show that higher conductor material thickness until exceeding the skin depth leads to improved gain and signal transmission intensity, indicating good radiation efficiency. All measured results highlight the importance of having a conductor material thickness greater than the skin depth for achieving optimal performance in RF microwave devices, providing valuable guidance for the application of new materials in electronics.

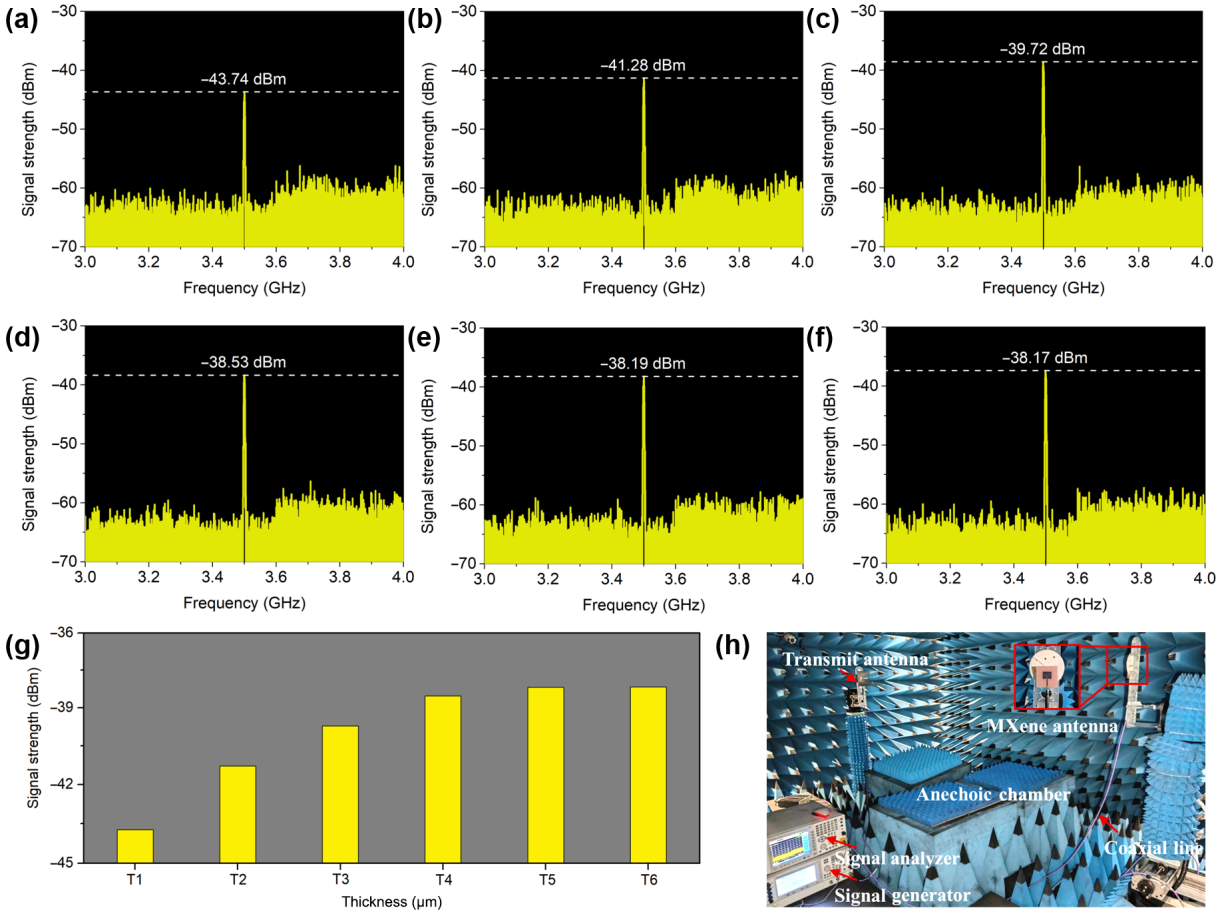

Figure 5 Signal transmission strength of MXene antennas. Signal intensity of MXene antenna with thickness of (a) T1, (b) T2, (c) T3, (d) T4, (e) T5, (f) T6, and (g) the comparition of T1–T6. (h) Measurement environment of MXene antenna signal intensity.

Acknowledgements

This work was supported by the National Natural Science Foundation of China (No. 51672204).

Electronic Supplementary Material: Supplementary material (the surface resistance and conductivity of MXene film, the digital photo of microstrip transmission line, the structure and dimensions of microstrip patch antenna, measurement environment of antenna performances, measured peak gain of MXene antennas, summary of conductivity of common new conductive materials) is available in the online version of this article at https://doi.org/10.1007/s12274-023-6127-7.

References

[1] Zhao, W. W.; Ni, H.; Ding, C. B.; Liu, L. L.; Fu, Q. F.; Lin, F. F.; Tian, F.; Yang, P.; Liu, S. J.; He, W. J. et al. 2D titanium carbide printed flexible ultrawideband monopole antenna for wireless communications. *Nat. Commun.* **2023**, *14*, 278.

[2] Hussain, R. Shared-aperture slot-based sub-6-GHz and mm-wave IoT antenna for 5G applications. *IEEE Internet Things J.* **2021**, *8*, 10807–10814.

[3] Zhang, L.; Zhang, J. X.; He, Y. J.; Mao, C. X.; Li, W. T.; Wong, S. W.; Mei, P.; Gao, S. A single-layer 10–30 GHz reflectarray antenna for the internet of vehicles. *IEEE Trans. Veh. Technol.* **2022**, *71*, 1480–1490.

[4] Dorrah, A. H.; Eleftheriades, G. V. Experimental demonstration of peripherally-excited antenna arrays. *Nat. Commun.* **2021**, *12*, 6109.

[5] Tian, X.; Lee, P. M.; Tan, Y. J.; Wu, T. L. Y.; Yao, H. C.; Zhang, M. Y.; Li, Z. P.; Ng, K. A.; Tee, B. C. K.; Ho, J. S. Wireless body sensor networks based on metamaterial textiles. *Nat. Electron.* **2019**, *2*, 243–251.

[6] Ibrahim, A. A.; Mohamed, H. A.; Abdelghany, M. A.; Tammam, E. Flexible and frequency reconfigurable CPW-fed monopole antenna with frequency selective surface for IoT applications. *Sci. Rep.* **2023**, *13*, 8409.

[7] Hu, P. F.; Leung, K. W.; Luk, K. M.; Pan, Y. M.; Zheng, S. Y. Diversity glass antennas for Tri-band WiFi applications. *Engineering* **2023**, *23*, 157–169.

[8] Pei, R.; Leach, M. P.; Lim, E. G.; Wang, Z.; Song, C. Y.; Wang, J. C.; Zhang, W. Z.; Jiang, Z. Z.; Huang, Y. Wearable EBG-backed belt antenna for smart on-body applications. *IEEE Trans. Industr. Inform.* **2020**, *16*, 7177–7189.

[9] Baumbauer, C. L.; Anderson, M. G.; Ting, J.; Sreekumar, A.; Rabaey, J. M.; Arias, A. C.; Thielens, A. Printed, flexible, compact UHF-RFID sensor tags enabled by hybrid electronics. *Sci. Rep.* **2020**, *10*, 16543.

[10] Lim, E. G.; Wang, J. C.; Juans, G.; Wang, Z.; Leach, M. P.; Lee, S.; Theera-Umpon, N. Design of wearable radio frequency identification antenna. *Wireless Pers. Commun.* **2018**, *98*, 3059–3070.

[11] I, C. L.; Han, S. F.; Bian, S. Energy-efficient 5G for a greener future. *Nat. Electron.* **2020**, *3*, 182–184.

[12] Asci, C.; Sadeqi, A.; Wang, W.; Rezaei Nejad, H.; Sonkusale, S. Design and implementation of magnetically-tunable quad-band filter utilizing split-ring resonators at microwave frequencies. *Sci. Rep.* **2020**, *10*, 1050.

[13] Kaim, V.; Kanaujia, B. K.; Kumar, S.; Choi, H. C.; Kim, K. W.; Rambabu, K. Ultra-miniature circularly polarized CPW-fed implantable antenna design and its validation for biotelemetry applications. *Sci. Rep.* **2020**, *10*, 6795.

[14] Ferrari, A. C.; Bonaccorso, F.; Fal'Ko, V.; Novoselov, K. S.; Roche, S.; Boggild, P.; Borini, S.; Koppens, F. H. L.; Palermo, V.; Pugno, N. et al. Science and technology roadmap for graphene, related two-dimensional crystals, and hybrid systems. *Nanoscale* **2015**, *7*, 4598–4810.

[15] Guna, V. K.; Murugesan, G.; Basavarajaiah, B. H.; Ilangovan, M.; Olivera, S.; Krishna, V.; Reddy, N. Plant-based completely

biodegradable printed circuit boards. *IEEE Trans. Electron Devices* **2016**, *63*, 4893–4898.
[16] Awasthi, A. K.; Li, J. H.; Koh, L.; Ogunseitan, O. A. Circular economy and electronic waste. *Nat. Electron.* **2019**, *2*, 86–89.
[17] Song, R. G.; Jiang, S. Q.; Hu, Z. L.; Fan, C.; Li, P.; Ge, Q.; Mao, B. Y.; He, D. P. Ultra-high conductive graphene assembled film for millimeter wave electromagnetic protection. *Sci. Bull.* **2022**, *67*, 1122–1125.
[18] Song, R. G.; Wang, Z.; Zu, H. R.; Chen, Q.; Mao, B. Y.; Wu, Z. P.; He, D. P. Wideband and low sidelobe graphene antenna array for 5G applications. *Sci. Bull.* **2021**, *66*, 103–106.
[19] Shao, Y. Z.; Wei, L. S.; Wu, X. Y.; Jiang, C. M.; Yao, Y.; Peng, B.; Chen, H.; Huangfu, J. T.; Ying, Y. B.; Zhang, C. J. et al. Room-temperature high-precision printing of flexible wireless electronics based on MXene inks. *Nat. Commun.* **2022**, *13*, 3223.
[20] Puchades, I.; Rossi, J. E.; Cress, C. D.; Naglich, E.; Landi, B. J. Carbon nanotube thin-film antennas. *ACS Appl. Mater. Interfaces* **2016**, *8*, 20986–20992.
[21] Amram Bengio, E.; Senic, D.; Taylor, L. W.; Headrick, R. J.; King, M.; Chen, P. Y.; Little, C. A.; Ladbury, J.; Long, C. J.; Holloway, C. L. et al. Carbon nanotube thin film patch antennas for wireless communications. *Appl. Phys. Lett.* **2019**, *114*, 203102.
[22] Guan, H. J.; Song, R. G.; Tong, C.; Zhao, X.; Yang, Y. P.; He, D. P. Graphene assembled film based conformal sensor array for submillimeter crack location and direction detection. *Appl. Phys. Express* **2023**, *16*, 015512.
[23] Zhang, J. W.; Wang, Y. C.; Song, R. G.; Kou, Z. K.; He, D. P. Highly flexible graphene-film-based rectenna for wireless energy harvesting. *Energy Environ. Mater.*, in press, DOI: 10.1002/eem2.12548.
[24] Zu, H. R.; Wu, B.; Zhang, Y. H.; Zhao, Y. T.; Song, R. G.; He, D. P. Circularly polarized wearable antenna with low profile and low specific absorption rate using highly conductive graphene film. *IEEE Antennas Wirel. Propag. Lett.* **2020**, *19*, 2354–2358.
[25] Li, Y.; Tian, X.; Gao, S. P.; Jing, L.; Li, K. R.; Yang, H. T.; Fu, F. F.; Lee, J. Y.; Guo, Y. X.; Ho, J. S. et al. Reversible crumpling of 2D titanium carbide (MXene) nanocoatings for stretchable electromagnetic shielding and wearable wireless communication. *Adv. Funct. Mater.* **2020**, *30*, 1907451.
[26] Han, M. K.; Liu, Y. Q.; Rakhmanov, R.; Israel, C.; Tajin, M. A. S.; Friedman, G.; Volman, V.; Hoorfar, A.; Dandekar, K. R.; Gogotsi, Y. Solution-processed $Ti_3C_2T_x$ MXene antennas for radio-frequency communication. *Adv. Mater.* **2021**, *33*, e2003225.
[27] Song, R. G.; Wang, Q. L.; Mao, B. Y.; Wang, Z.; Tang, D. L.; Zhang, B.; Zhang, J. W.; Liu, C. G.; He, D. P.; Wu, Z. et al. Flexible graphite films with high conductivity for radio-frequency antennas. *Carbon* **2018**, *130*, 164–169.
[28] Pan, K. W.; Fan, Y. Y.; Leng, T.; Li, J. S.; Xin, Z. Y.; Zhang, J. W.; Hao, L.; Gallop, J.; Novoselov, K. S.; Hu, Z. R. Sustainable production of highly conductive multilayer graphene ink for wireless connectivity and IoT applications. *Nat. Commun.* **2018**, *9*, 5197.
[29] Hui, Y. Y.; Zu, H. R.; Song, R. G.; Fu, H. Q.; Luo, K. L.; Tian, C.; Wu, B.; Huang, G. L.; Kou, Z. K.; Cheng, X. et al. Graphene-assembled film-based reconfigurable filtering antenna with enhanced corrosion-resistance. *Crystals* **2023**, *13*, 747.
[30] Jiang, S. Q.; Song, R. G.; Hu, Z. L.; Xin, Y. T.; Huang, G. L.; He, D. P. Millimeter wave phased array antenna based on highly conductive graphene-assembled film for 5G applications. *Carbon* **2022**, *196*, 493–498.
[31] Song, R. G.; Mao, B. Y.; Wang, Z.; Hui, Y. Y.; Zhang, N.; Fang, R.; Zhang, J. W.; Wu, Y. E.; Ge, Q.; Novoselov, K. S. et al. Comparison of copper and graphene-assembled films in 5G wireless communication and THz electromagnetic-interference shielding. *Proc. Natl. Acad. Sci. USA* **2023**, *120*, e2209807120.
[32] Szeftel, J.; Sandeau, N.; Khater, A. Study of the skin effect in superconducting materials. *Phys. Lett. A* **2017**, *381*, 1525–1528.
[33] Zhao, M. Q.; Trainor, N.; Ren, C. E.; Torelli, M.; Anasori, B.; Gogotsi, Y. Scalable manufacturing of large and flexible sheets of MXene/graphene heterostructures. *Adv. Mater. Technol.* **2019**, *4*, 1800639.
[34] Song, R. G.; Zhao, X.; Wang, Z.; Fu, H. Q.; Han, K. K.; Qian, W.; Wang, S. Y.; Shen, J.; Mao, B. Y.; He, D. P. Sandwiched graphene clad laminate: A binder-free flexible printed circuit board for 5G antenna application. *Adv. Eng. Mater.* **2020**, *22*, 2000451.
[35] Si, Y. F.; Jin, H. H.; Zhang, Q.; Xu, D. W.; Xu, R. X.; Ding, A. X.; Liu, D. Roll-to-roll processable MXene-rGO-PVA composite films with enhanced mechanical properties and environmental stability for electromagnetic interference shielding. *Ceram. Int.* **2022**, *48*, 24898–24905.
[36] Wang, H.; Cui, Z.; He, S. A.; Zhu, J. Q.; Luo, W.; Liu, Q.; Zou, R. J. Construction of ultrathin layered MXene-TiN heterostructure enabling favorable catalytic ability for high-areal-capacity lithium-sulfur batteries. *Nano-Micro Lett.* **2022**, *14*, 189.
[37] Hao, S. W.; Fu, Q. J.; Meng, L.; Xu, F.; Yang, J. A biomimetic laminated strategy enabled strain-interference free and durable flexible thermistor electronics. *Nat. Commun.* **2022**, *13*, 6472.